

RAPID COMMUNICATION

Magneto-optical trap for neutral mercury atoms

To cite this article: Liu Hong-Li *et al* 2013 *Chinese Phys. B* **22** 043701

View the [article online](#) for updates and enhancements.

You may also like

- [Cavity enhanced measurement of trap frequency in an optical dipole trap](#)
Peng-Fei Yang, , Hai He et al.
- [Metal-inorganic frameworks with pnictogen linkers](#)
Tatiana A. Shestimerova and Andrei V. Shevelkov
- [Testing the Universality of Free Fall by Comparing the Atoms in Different Hyperfine States with Bragg Diffraction](#)
Ke Zhang, , Min-Kang Zhou et al.

Magneto-optical trap for neutral mercury atoms*

Liu Hong-Li(刘洪力)^{a)}, Yin Shi-Qi(尹士奇)^{a)}, Liu Kang-Kang(刘亢亢)^{a)}, Qian Jun(钱 军)^{a)},
Xu Zhen(徐 震)^{a)†}, Hong Tao(洪 涛)^{b)}, and Wang Yu-Zhu(王育竹)^{a)b)‡}

^{a)}Key Laboratory for Quantum Optics, Shanghai Institute of Optics and Fine Mechanics, Chinese Academy of Sciences, Shanghai 201800, China

^{b)}Center for Macroscopic Quantum Phenomena, Shanghai Advanced Research Institute, Chinese Academy of Sciences, Shanghai 201210, China

(Received 26 October 2012; revised manuscript received 4 December 2012)

Due to its low sensitivity to blackbody radiation, neutral mercury is a good candidate for the most accurate optical lattice clock. Here we report the observation of cold mercury atoms in a magneto-optical trap (MOT). Because of the high vapor pressure at room temperature, the mercury source and the cold pump were cooled down to $-40\text{ }^{\circ}\text{C}$ and $-70\text{ }^{\circ}\text{C}$, respectively, to keep the science chamber in an ultra-high vacuum of 6×10^{-9} Pa. Limited by the power of the UV cooling laser, the one beam folded MOT configuration was adopted, and 1.5×10^5 Hg-202 atoms were observed by fluorescence detection.

Keywords: laser cooling and trapping, neutral mercury atom, laser spectroscopy

PACS: 37.10.Gh, 37.10.De, 32.30.Jc

DOI: 10.1088/1674-1056/22/4/043701

1. Introduction

Recently, the performance of the optical atomic clock has largely surpassed that of microwave fountain clocks.^[1–4] Compared with the optical clock with a single ion, the optical lattice clock with neutral atoms has a better signal to noise ratio (SNR).^[5–8] However, one of the fundamental limitations of the performance of the optical lattice clock is the black body radiation (BBR) shift.^[9] The fractional uncertainties of the BBR shift for strontium (Sr) and ytterbium (Yb) are 7×10^{-17} and 3×10^{-16} , respectively.^[9] Mercury (Hg) with a low sensitivity to BBR has been regarded as a good candidate for the most accurate optical lattice clock.^[10] As the heaviest non-radioactive atom that can be laser-cooled,^[10–12] the mercury atom has the advantages of testing the variation of fundamental constants^[13] and the *CP* violation of permanent electric dipole moments (EDM).^[14] So far, several groups have reported the observation of the mercury magneto-optical trap (MOT).^[10–12] Furthermore, the clock transition,^[11] the narrow Lamb-Dicke spectroscopy, and the magic wavelength of the lattice laser^[15] have been measured. Very recently, the absolute clock frequency (Hg-199) with a fraction uncertainty of 5.7×10^{-15} has been reported.^[16]

This paper is organized as follows. In Section 2, we briefly introduce the properties of neutral mercury atoms. In Section 3, our experimental setup of the MOT is described in detail. Finally, we present the experimental results on the observation of the trapped mercury atoms.

2. Properties of neutral mercury atoms

Mercury has seven natural stable isotopes, two fermions (Hg-199, Hg-201) and five bosons (Hg-196, Hg-198, Hg-200, Hg-202, Hg-204). The mercury atom has an electronic structure and an energy level structure similar to those of Sr and Yb, as shown in Fig. 1. In principle, three transitions can be used for Doppler laser cooling, the singlet transition between $^1\text{S}_0$ and $^1\text{P}_1$ (184.9 nm), the intercombination transition between $^1\text{S}_0$ and $^3\text{P}_1$ (253.7 nm),^[17] and the transition between the meta-stable state $^3\text{P}_2$ and state $^3\text{D}_2$ (365 nm). For Sr and Yb atoms, thermal atoms are first slowed by a Zeeman slower due to the strong singlet transition ($^1\text{S}_0\text{--}^1\text{P}_1$), and are then loaded into an MOT operated with the intercombination transition ($^1\text{S}_0\text{--}^3\text{P}_1$).^[18–21] The two-cascade cooling technique, however, cannot be used for Hg atoms because the singlet transition $^1\text{S}_0\text{--}^1\text{P}_1$ has a large linewidth (120 MHz) and a deep-UV wavelength (185 nm). Therefore, the intercombination transition is used for MOT loading with a linewidth $2\pi\times 1.27$ MHz, saturation intensity 10.2 mW/cm^2 , and Doppler limited temperature $30\text{ }\mu\text{K}$. Due to no fine or hyperfine splitting in the ground state, the repumping laser is not required in the laser cooling of mercury atoms.

The high vapor pressure of mercury (0.3 Pa at room temperature^[22]) makes the mercury source easy to obtain, which can reach a high optical density with a few-mm-long cell. Compared with other metal atomic gases, no heating is required, and the mercury source should be cooled below $-50\text{ }^{\circ}\text{C}$ and kept at ultra-high vacuum.^[10–12,23]

*Project supported by the Research Project of Shanghai Science and Technology Commission, China (Grant No. 09DJ1400700), the National Natural Science Foundation of China (Grant Nos. 10974211 and 11104292), and the National Basic Research Program of China (Grant No. 2011CB921504).

†Corresponding author. E-mail: xuzhen@siom.ac.cn

‡Corresponding author. E-mail: yzwang@mail.shcnc.ac.cn

© 2013 Chinese Physical Society and IOP Publishing Ltd

<http://iopscience.iop.org/cpb> <http://cpb.iphy.ac.cn>

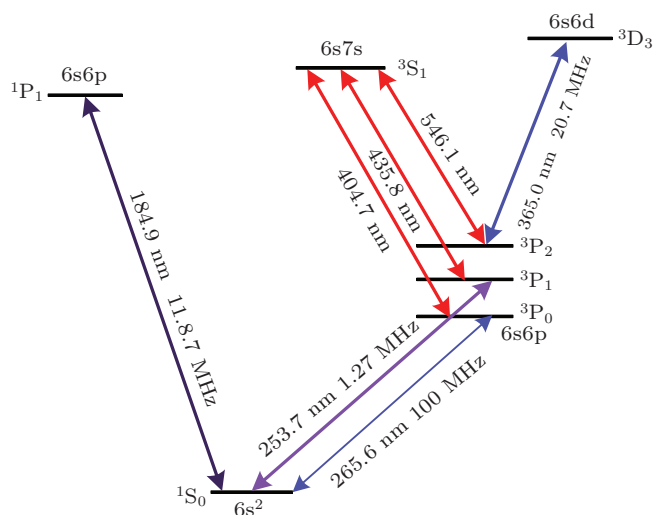


Fig. 1. (color online) Energy level diagram of Hg. The transitions of 1S_0 – 3P_1 and 1S_0 – 3P_0 are used for cooling and clock transitions, respectively.

3. Experimental setup of the magneto-optical trap for neutral mercury atoms

The vacuum system consists of two chambers, a source chamber and a main chamber, which are linked by a gate valve. The thermoelectric cooled mercury source is the key component in the source chamber, which is shown in Fig. 2. The mercury cup is cooled by a multi-stage thermoelectric cooler (TEC), and the TEC is glued onto a water cooled heat sink. When the temperature of water is kept at 10 °C, the mercury cup can be cooled to –80 °C. For daily operation, the cup cools down to –70 °C. For MOT operation, the temperature is kept at –50 °C, which corresponds to mercury's vapor pressure of 3.5×10^{-5} Pa.

The science chamber has eight indium-sealed UV-fused silica (UVFS) windows with anti-reflection coatings at 254 nm, six of them for MOT beam access, and two for detection and monitoring. An ion pump and a cold pump are placed at the end of the science chamber to keep a vacuum of 2×10^{-8} Pa when the gate valve is closed. The cold pump is used to collect the background mercury atoms, which has a pump speed of 47 L/s for mercury when the plate temperature is –70 °C. When the gate valve is open, the vacuum of the science chamber raises to 8×10^{-7} Pa (2×10^{-6} Pa) as the source chamber works at –70 °C (–50 °C). A pair of anti-Helmholtz coils are mounted on the two sides of the science chamber to generate a quadruple magnetic field with an axial magnetic field gradient of 5.38 Gs/(cm·A) along the gravity ($1 \text{ Gs} = 10^{-4} \text{ T}$).

A commercial diode laser system (Toptica TA-FHG-1030) is used to generate the cooling laser. The seed laser operates at 1014.9 nm with a linewidth smaller than 150 kHz. The laser is amplified to 1 W by a semiconductor taper amplifier. After two cascaded stages of cavity enhanced frequency doubling with LBO and BBO crystals, the output power is

about 30 mW at 253.7 nm. The output UV laser is split to two beams by a polarization beam splitter (PBS), one for saturated absorption spectroscopy (3 mW), and the other for laser cooling (25 mW).

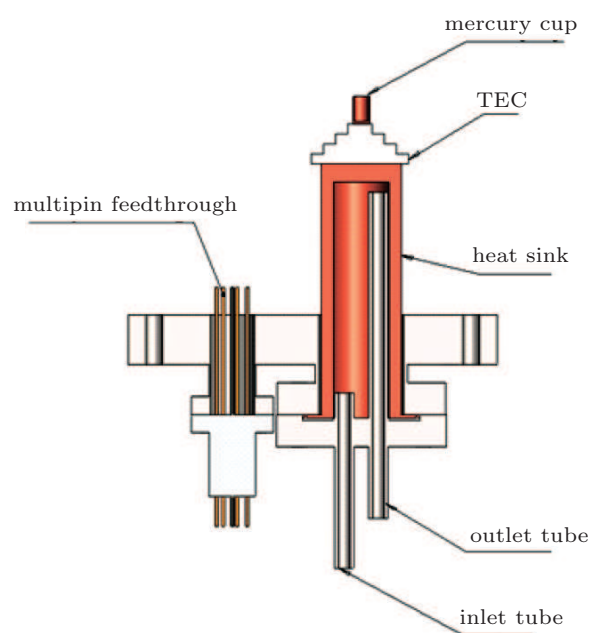


Fig. 2. (color online) Schematic diagram of the TEC cooled mercury source and cold pump. Two Pt100s are glued on the cup and the heat sink respectively. The heat sink, which is silver-plated to prevent the corrosion of the water, has a ring configuration in the bottom served as the gasket. For the cold pump in the main chamber, the OFC cup is replaced with a 15-mm×20-mm×2-mm OFC plate.

The schematic diagram of the saturated absorption spectroscopy (SAS) is shown in Fig. 3. A home-made 2-mm-length UVFS mercury cell is used. The powers of the pump and the probe lasers are 2 mW and 0.4 mW, respectively, and they have the same diameter of 2 mm. Because of the high vapor pressure at room temperature, the SAS can be realized by using a few-millimeter cell, this can make the setup of SAS for mercury much smaller.

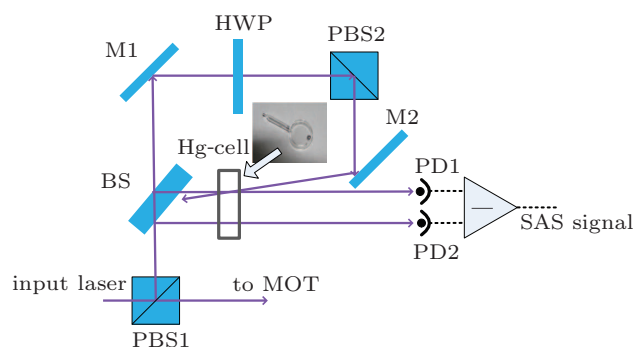


Fig. 3. (color online) Schematic diagram of saturated absorption spectroscopy. Here M stands for mirror, PBS for polarization beam splitter, BS for beam splitter, HWP for half wavelength plate; PDs for photodiode detectors (Hamamatsu, S1336). The Hg-cell is a 2-mm long cell made of UVFS; the differential signal is used to enhance the SNR.

The cooling beam is magnified to 15 mm in e^{-2} diameter by a Kepler telescope. To save the UV power, we use the folded cooling beam with one shot for the MOT. We use the fluorescence imaging method to detect the MOT signal. In order to enhance the signal-to-noise ratio, we use two stages of spatial filters with two lens and two irises to avoid the background scattering light, as depicted in Fig. 4. The MOT signal is detected by a photomultiplier tube (PMT, Hamamatsu, H9305-01) or an alternative electron multiplying CCD (EMCCD, Andor, iXon3 885). The signal from the PMT is amplified by a low-current amplifier (SRS, SR570) to count the atom number. The shape and the size of the atomic cloud are recorded by the EMCCD. In our imaging system, the fluorescence collection efficiency is 0.1%, and the magnification is 0.5. The cathode radiant sensitivity of the PMT is 60 mA/W at 254 nm.

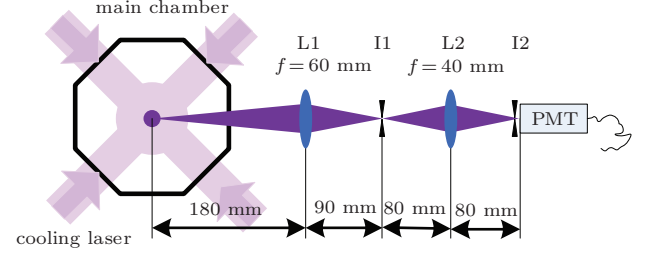


Fig. 4. (color online) Schematic diagram of the fluorescence imaging system. Here L1 and L2 are the imaging lenses with focal lengths of 60 mm and 40 mm, respectively; I1 and I2 are the irises for the spatial filter.

4. Results

Now we present our main experimental results. First we observe the SAS signals of several mercury isotopes, as shown in Fig. 5. Due to the isotope abundance, the signals for Hg-202 and Hg-200 are much better. The SAS signal is used to discriminate the frequency of the UV laser in our experiment.

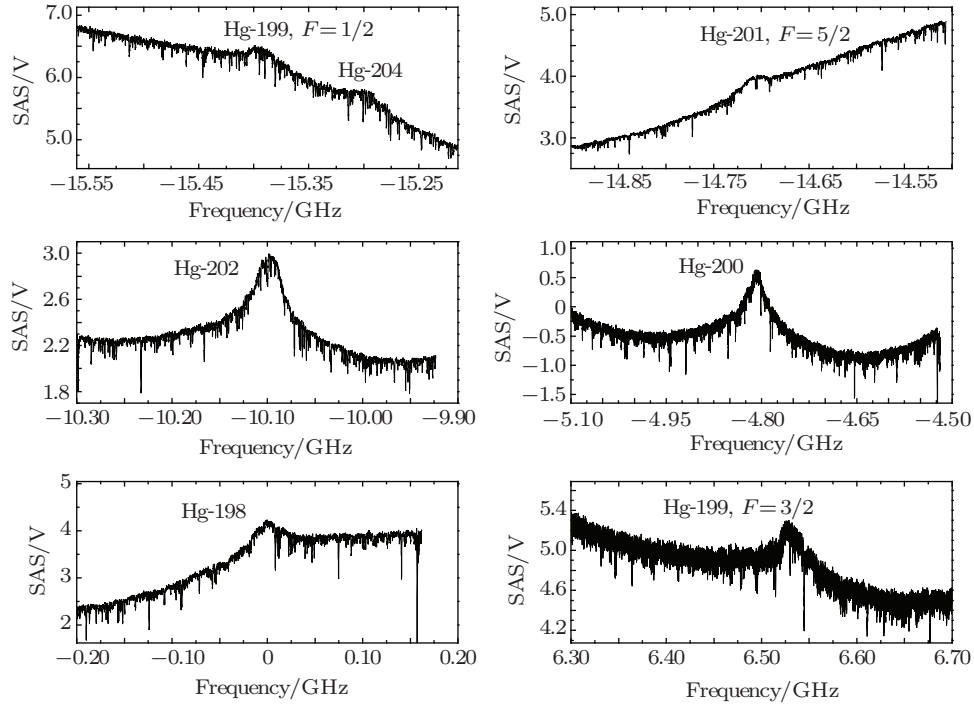


Fig. 5. SAS signals of the $1S_0$ to $3P_1$ transition for several Hg isotopes.

Because the laser frequency cannot be locked on the $1S_0-3P_1$ transition in our experiment, we slowly sweep the UV laser across the resonance of Hg-202 with 5.3 MHz/s to find the MOT signal, and simultaneously monitor the laser frequency by the SAS signal. Limited by the waist of the cooling beam being 7 mm, the capture velocity is about 5.9 m/s for the $1S_0-3P_1$ transition. The optimized axial magnetic field gradient is 13 Gs/cm, and the intensity of the cooling laser is about 13 mW/cm^2 ($1.3I_{\text{sat}}$). The fluorescence signal is collected by the PMT and shown in Fig. 6. It is clear that the atoms are

loaded in the MOT when the laser is red-detuned. The sharp falling edge of the MOT signal indicates the resonance of Hg-202. The fluorescence images are also taken from the EMCCD, as shown in the inset of Fig. 6. In this image, the diameters of the cold mercury atoms are 0.74 mm and 0.96 mm in the vertical and horizontal directions, respectively.

The atom number in the MOT, N_{MOT} , can be derived from the PMT signal as

$$N_{\text{MOT}} = U_{\text{PMT}} / \left(\Gamma_{\text{sc}} h \nu \eta_{\text{det}} T \eta_{\text{PMT}} \frac{G_{\text{PMT}}}{S_{\text{amp}}} \right), \quad (1)$$

where U_{PMT} is the PMT signal in units of V, $h\nu$ is the single photon energy (253.7 nm), η_{PMT} is the cathode radiant sensitivity of the PMT (60 mA/W), is the gain of the PMT which is set to 2×10^4 , S_{amp} is the sensitivity of the SR570 (500 nA/V), G_{PMT} is the fluorescence collection efficiency 0.001, T is the transmission coefficient of the imaging system (90%), and Γ_{sc} is the scattering rate, i.e.

$$\Gamma_{\text{sc}} = \frac{\Gamma}{2} \frac{I(r)/I_{\text{sat}}}{1 + I(r)/I_{\text{sat}} + 4(\Delta)^2/\Gamma^2}. \quad (2)$$

By considering the sharp edge and the sweep rate, we can estimate that the detuning is about 0.1 MHz–0.5 MHz at the peak of the PMT signal. The mercury-atom number is estimated to be 1.5×10^5 in the MOT, and the atomic density is about 4.2×10^8 atom/cm³.

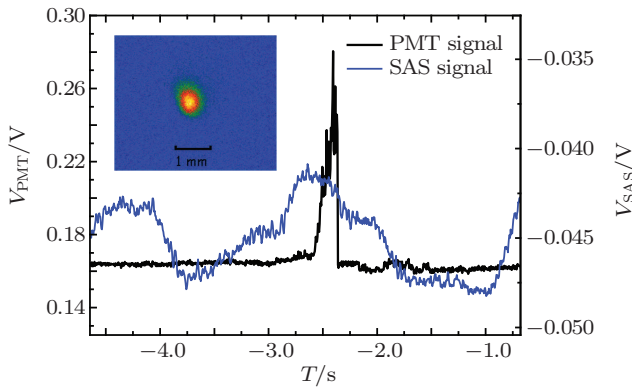


Fig. 6. (color online) PMT and SAS signals of Hg-202. The UV laser is swept across the resonance of Hg-202 at 5.3 MHz/s. The inset is the image of the MOT taken from the EMCCD.

5. Conclusion

In conclusion, we observe approximately 1.5×10^5 atoms of Hg-202 in a magneto-optical trap with one beam folded configuration. The UV cooling laser is discriminated by saturated absorption spectroscopy, and the fluorescence signal is detected by a two-stage spatial filtered imaging system. The vacuum of the science chamber can be kept at 2×10^{-8} Pa with the TEC-cooled mercury source and the cold pump at -70 °C.

Acknowledgements

The authors thank Shen Guo-Jian for manufacturing the mercury cells, Duan Ya-Fan for experimental assistance, and Wu Hai-Bin and Xu Da-Min for their technical support.

References

- [1] Chou C W, Hume D B, Koelemeij J C J, Wineland D J and Rosenband T 2010 *Phys. Rev. Lett.* **104** 070802
- [2] Rosenband T, Hume D B, Schmidt P O, Chou C W, Brusch A, Lorini L, Oskay W H, Drullinger R E, Fortier T M, Stalnaker J E, Diddams S A, Swann W C, Newbury N R, Itano W M, Wineland D J and Bergquist J C 2008 *Science* **319** 1808
- [3] Lemke N D, Ludlow A D, Barber Z W, Fortier T M, Diddams S A, Jiang Y, Jefferts S R, Heavner T P, Parker T E and Oates C W 2009 *Phys. Rev. Lett.* **103** 063001
- [4] Ludlow A D, Zelevinsky T, Campbell G K, Blatt S, Boyd M M, de Miranda M H G, Martin M J, Thomsen J W, Foreman S M, Ye J, Fortier T M, Stalnaker J E, Diddams S A, Le Coq Y, Barber Z W, Poli N, Lemke N D, Beck K M and Oates C W 2008 *Science* **319** 1805
- [5] Le Targat R, Baillard X, Fouche M, Brusch A, Tcherbakoff O, Rovera G D and Lemonde P 2006 *Phys. Rev. Lett.* **97** 130801
- [6] Takamoto M, Takano T and Katori H 2011 *Nat. Photon.* **5** 288
- [7] Katori H, Takamoto M, Pal'chikov V G and Ovsiannikov V D 2003 *Phys. Rev. Lett.* **91** 173005
- [8] Takamoto M, Hong F L, Higashi R and Katori H 2005 *Nature* **435** 321
- [9] Porsev S G and Derevianko A 2006 *Phys. Rev. A* **74** 020502
- [10] Hachisu H, Miyagishi K, Porsev S G, Derevianko A, Ovsiannikov V D, Pal'chikov V G, Takamoto M and Katori H 2008 *Phys. Rev. Lett.* **100** 053001
- [11] Petersen M, Chicireanu R, Dawkins S T, Magalhaes D V, Mandache C, Le Coq Y, Clairon A and Bize S 2008 *Phys. Rev. Lett.* **101** 183004
- [12] Villwock P, Siol S and Walther T 2011 *Eur. Phys. J. D* **65** 251
- [13] Angstrom E J, Dzuba V A and Flambaum V V 2004 *Phys. Rev. A* **70** 014102
- [14] Romalis M V, Griffith W C, Jacobs J P and Fortson E N 2001 *Phys. Rev. Lett.* **86** 2505
- [15] Yi L, Mejri S, McFerran J J, Le Coq Y and Bize S 2011 *Phys. Rev. Lett.* **106** 073005
- [16] McFerran J J, Yi L, Mejri S, Di Manno S, Zhang W, Guena J, Le Coq Y and Bize S 2012 *Phys. Rev. Lett.* **108** 183004
- [17] Yin S, Liu H, Qian J, Hong T, Xu Z and Wang Y 2012 *Opt. Commun.* **285** 5169
- [18] Zhao P, Xiong Z, Liang J, He L and Lü B 2008 *Chin. Phys. Lett.* **25** 3631
- [19] Zhao P, Xiong Z, Long Y, He L and Lü B 2009 *Chin. Phys. Lett.* **26** 083702
- [20] Wang S, Wang Q, Lin Y, Wang M, Lin B, Zang E, Li T and Fang Z 2009 *Chin. Phys. Lett.* **26** 093202
- [21] Wang Q, Lin B, Zhao Y, Li Y, Wang S, Wang M, Zang E, Li T and Fang Z 2011 *Chin. Phys. Lett.* **28** 033201
- [22] Lide D R 2009 *CRC Handbook of Chemistry and Physics* 90th edn. (Boca Raton: CRC Press)
- [23] McFerran J J, Yi L, Mejri S and Bize S 2010 *Opt. Lett.* **35** 3078